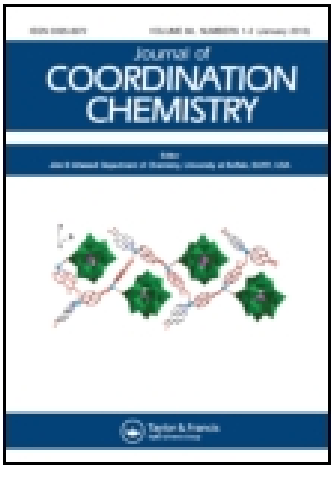

Journal of Coordination Chemistry
Publication details, including instructions for authors and subscription information:
http://www.tandfonline.com/loi/gcoo20

Synthesis, characterization, and computational study of three-coordinate SNS-copper(I) complexes based on bis-thione precursors

John R. Miecznikowski[a], Matthew A. Lynn[b], Jerry P. Jasinski[c], Eric Reinheimer[d], Daniel W. Bak[e], Mekhala Pati[e], Elizabeth E. Butrick[a], Anne Elise R. Drozdoski[a], Kerry A. Archer[a], Christine E. Villa[a], Elise G. Lemons[a], Erin Powers[a], Margaret Siu[a], Camile D. Gomes[a] & Kaitlyn N. Morio[a]

[a] Department of Chemistry and Biochemistry, Fairfield University, Fairfield, CT, USA

[b] Department of Science and Mathematics, National Technical Institute for the Deaf, Rochester Institute of Technology, Rochester, NY, USA

[c] Department of Chemistry, Keene State College, Keene, NH, USA

[d] Department of Chemistry, California State Polytechnic University Pomona, Pomona, CA, USA

[e] Department of Chemistry and Molecular Biology, Cell Biology, and Biochemistry, Boston University, Boston, MA, USA

Accepted author version posted online: 15 Jan 2014.Published online: 24 Feb 2014.

To cite this article: John R. Miecznikowski, Matthew A. Lynn, Jerry P. Jasinski, Eric Reinheimer, Daniel W. Bak, Mekhala Pati, Elizabeth E. Butrick, Anne Elise R. Drozdoski, Kerry A. Archer, Christine E. Villa, Elise G. Lemons, Erin Powers, Margaret Siu, Camile D. Gomes & Kaitlyn N. Morio (2014) Synthesis, characterization, and computational study of three-coordinate SNS-copper(I) complexes based on bis-thione precursors, Journal of Coordination Chemistry, 67:1, 29-44, DOI: 10.1080/00958972.2014.883070

To link to this article: http://dx.doi.org/10.1080/00958972.2014.883070

Journal of Coordination Chemistry, 2014
Vol. 67, No. 1, 29–44, http://dx.doi.org/10.1080/00958972.2014.883070

Synthesis, characterization, and computational study of three-coordinate SNS-copper(I) complexes based on bis-thione precursors

JOHN R. MIECZNIKOWSKI*†, MATTHEW A. LYNN‡, JERRY P. JASINSKI§, ERIC REINHEIMER¶, DANIEL W. BAK‖, MEKHALA PATI‖ ELIZABETH E. BUTRICK†, ANNE ELISE R. DROZDOSKI†, KERRY A. ARCHER†, CHRISTINE E. VILLA†, ELISE G. LEMONS†, ERIN POWERS†, MARGARET SIU†, CAMILE D. GOMES† and KAITLYN N. MORIO†

†Department of Chemistry and Biochemistry, Fairfield University, Fairfield, CT, USA
‡Department of Science and Mathematics, National Technical Institute for the Deaf, Rochester Institute of Technology, Rochester, NY, USA
§Department of Chemistry, Keene State College, Keene, NH, USA
¶Department of Chemistry, California State Polytechnic University Pomona, Pomona, CA, USA
‖Department of Chemistry and Molecular Biology, Cell Biology, and Biochemistry, Boston University, Boston, MA, USA

(*Received 1 November 2013; accepted 30 December 2013*)

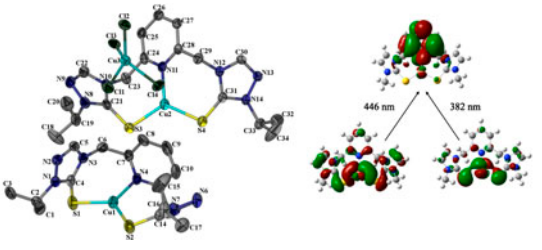

A series of tridentate pincer ligands, each possessing two sulfur and one nitrogen donor (SNS), based on bis-imidazolyl or bis-triazolyl salts were metallated with $CuCl_2$ to give new tridentate SNS pincer copper(I) complexes $[(SNS)Cu]^+$. These orange complexes exhibit a three-coordinate pseudo-trigonal-planar geometry in copper. During the formation of these copper(I) complexes, disproportionation is observed as the copper(II) salt precursor is converted into the Cu(I) $[(SNS)Cu]^+$ cation and the $[CuCl_4]^{2-}$ counteranion. The $[(SNS)Cu]^+$ complexes were characterized with single crystal X-ray diffraction, electrospray mass spectrometry, EPR spectroscopy, attenuated total reflectance infrared spectroscopy, UV–Vis spectroscopy, cyclic voltammetry, and elemental analysis. The EPR spectra are consistent with anisotropic Cu(II) signals with four hyperfine splittings in the lower-field region ($g_{||}$) and g values consistent with the presence of the tetrachlorocuprate. Various electronic transitions are apparent in the UV–Vis spectra of the complexes and originate in the

*Corresponding author. Email: jmiecznikowski@fairfield.edu

copper-containing cations and anions. Density functional calculations support the nature of the SNS binding, allowing assignment of a number of features present in the UV–Vis and IR spectra and cyclic voltammograms of these complexes.

Keywords: SNS pincer ligand; SNS Cu pincer complexes; X-ray crystallography; Cyclic voltammetry; Density functional theory calculations; EPR spectroscopy

1. Introduction

Recently, we reported a series of tridentate pincer ligand precursors possessing SNS donors [1, 2]. In our previous studies, we have used these ligands to gage the impact of ligand flexibility on the structure and catalytic reactivity of tridentate zinc(II) SNS pincer complexes. Through the fusion of variously substituted pyridine precursors with N-heterocycles, followed by reaction of the ligand precursor salt with sodium acetate and sulfur, SNS ligand systems with variable flexibility and electronic properties can be prepared (figure 1).

Using 2,6-dibromopyridine as a starting material permits the thioimidazolyl groups to bind directly to the pyridine moiety (**1a**–**c**). Such a ligand system is relatively stiff; rotation about the C–N bond that links the pyridinyl and imidazolyl moieties is the only way in which these rings can move relative to each other. We have also prepared SNS ligands with a greater degree of flexibility by employing 2,6-(dibromomethyl)pyridine, thereby introducing a methylene linker between the fragments (**2a**–**c** and **3a**–**c**). We were able to further fine-tune the electronic environment within the framework of these systems by using imidazolyl- (**2a**–**c**) and triazolyl- (**3a**–**c**) based precursors in the preparation of the pincer ligands. Use of these variously tuned tridentate ligand sets has allowed us to compare the effect of ligand flexibility on the reactivity of their zinc-bound complexes toward the catalytic reduction of electron-poor aldehydes [1, 2]. Jia and co-workers have prepared ligand precursor **1a** (figure 1) and used it to prepare half-sandwich iridium and rhodium complexes [3].

The preparation of ligands that contain nitrogen and sulfur donors, as well as of copper complexes that contain these ligands is of considerable interest in bioinorganic chemistry. In electron-transfer proteins, interactions between copper and the thiolate functionality of cysteine are important [4, 5]. Sulfide–copper interactions are also found in the Cu_4–S cluster in nitrous oxide reductase [6–8]. In addition, thioether–methionine–copper ion interactions occur in Type 1 "blue" electron-transfer proteins and in the active site of certain monooxygenases [9, 10].

Using the ligand precursors shown in figure 1, we focused attention in our current work on the preparation of SNS-bound copper complexes using ligand precursors **2a**, **3a**, and **3c** (figure 1). Of course, numerous three-coordinate mononuclear copper(I) [11–22] and copper (II) [23–27] complexes are known with various kinds of coordination observed at the metal

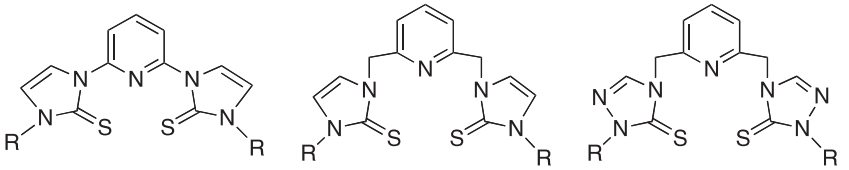

Figure 1. SNS ligand precursors previously prepared by Miecznikowski *et al.* [1, 2] and Jin *et al.* [3].

center. The Cu(I) complexes reported previously all exhibit pseudo-trigonal-planar geometry about copper. The three-coordinate copper(II) complexes possess either a pseudo-trigonal planar [23, 26] or a T-shaped coordination environment [24, 25] about the copper center. To the best of our knowledge, a three-coordinate copper complex with S, S, and N donors has not been reported. An iridium piano stool complex with a tridentate SSN ligand has been reported recently [28].

We present here the syntheses, X-ray crystallographic, spectroscopic, and electrochemical characterizations, and computational analysis of our new three-coordinate copper(I) complexes containing a tridentate ligand with two sulfur and one nitrogen donor.

2. Experimental

2.1. *General procedures*

All reagents used are commercially available and were used as received. All of the reagents and solvents were purchased from Acros Organics except for diethyl ether and sodium acetate, which were purchased from Fisher. We previously reported syntheses of the ligand precursors 2,6-bis{[N-butyl]imidazol-1-ylidene-2-thione}pyridine, 2,6-bis{[N-isopropyl]imidazol-1-ylidene-2-thione}pyridine,2,6-bis{[N-neopentyl]imidazol-1-ylidene-2-thione}pyridine, 2,6-bis{[N-isopropyl-N′-methylene]imidazol-1-ylidene-2-thione}pyridine, 2,6-bis{[N-isopropyl-N′-methylene]triazole-2-thione}pyridine and 2,6-bis{[N-butyl-N′-methylene]imidazol-1-ylidene-2-thione}pyridine used herein [1–3].

Each sample was analyzed by direct flow injection (injection volume = 3 or 10 µL) electro spray ionization (ESI) on a Waters Q-Tof API US instrument in the positive mode. The optimized conditions were: capillary = 3000 kV, cone = 10 or 35 V, source temperature = 120 °C and desolvation temperature = 120 or 350 °C.

Cyclic voltammetry experiments were performed using a Cypress Electroanalytical System with a silver wire reference electrode, a glassy carbon working electrode, and a platinum counterelectrode. The supporting electrolyte for the cyclic voltammetry experiments was tetra-N-butylammonium tetrafluoroborate. The solvent for the cyclic voltammetry experiments was DMSO. The ferrocenium/ferrocene couple was used as an internal reference; reduction potential values were corrected by assigning the ferrocenium/ferrocene couple to 0.40 V *versus* SCE.

IR spectra were collected using a Thermo Nicolet AVATAR 380 FT-IR with a SMART SPECULATR reflectance adaptor, or a Bruker Tensor 27 FT-IR with an attenuated total reflectance (ATR) adaptor. C, H, and N elemental analyses were performed by Atlantic Microlab Inc. (Norcross, GA).

Low-temperature (10 K) EPR measurements were made using a Bruker X-band ESEXSYS E 500 spectrometer equipped with an ESR900 continuous flow liquid helium cryostat. EPR spectra were collected at (9.24 GHz), (2 mW) microwave power and with a (1G) modulation amplitude. The EPR samples of the copper complexes were prepared by dissolving 3 mg of the copper complex in 0.8 mL of methanol. Spectra were collected of oxidized samples and required no reduction prior to data collection.

2.2. *Syntheses*

2.2.1. Bis-[(η^3-S,S,N)(2,6-bis){[N-isopropyl-N′-methylene]imidazole-1-ylidene-2-thione} pyridine copper(I) tetrachlorocuprate] (4). In a 25 mL round-bottomed flask, 2,6-bis

{[N-isopropyl-N′-methylene]imidazole-1-ylidene-2-thione}pyridine (0.0967 g, 0.000269 moles) was combined with $CuCl_2$ (0.0365 g, 0.000271 moles) and dissolved in dichloromethane (10 mL). The solution mixture was refluxed for 20 h. After this time, the solvent was removed under reduced pressure. Single crystals for elemental analyses were grown by slow vapor diffusion of diethyl ether into a methanol solution containing the copper complex. Yield: 0.12 g (69%). FT-IR (reflectance, solid crystal, ν_{max}/cm^{-1}, assignment): 3051 (br, C–H stretch), 2971 (br, C–H stretch). ESI MS (*m/z*): 450.0874 (450.08 Calcd for $[C_{19}H_{25}N_5S_2Cu]^+$). Elemental Anal. Calcd (found) for $[C_{19}H_{25}Cu_1N_5S_2]_2[CuCl_4]\cdot H_2O$: C, 40.55 (40.37); H, 4.66 (4.50); N, 12.44 (12.31). UV–Vis λ_{max} (CH_3CN)/nm ($\varepsilon/M^{-1}\,cm^{-1}$): 462 (260), 265 (36000), 204 (46000).

2.2.2. Bis[(η^3-S,S,N)(2,6-bis){[N-isopropyl-N′-methylene]triazole-2-thione} pyridine copper(I) tetrachlorocuprate] (5). In a 25 mL round-bottom flask, 2,6-bis{[N-isopropyl-N′-methylene]triazole-2-thione}pyridine (0.1491 g, 0.0003831 moles) was combined with $CuCl_2$ (0.0514 g, 0.000390 moles) and dissolved in dichloromethane (10 mL). The solution mixture was refluxed for 20 h and the solvent removed under reduced pressure. Single crystals for X-ray diffraction and elemental analyses were grown by slow vapor diffusion of diethyl ether into a methanol solution containing the copper complex. Yield: 0.16 g (64%). FT-IR (reflectance, solid crystal, ν_{max}/cm^{-1}, assignment): 3035 (br, C–H stretch), 2984 (br, C–H stretch), 2971 (br, C–H stretch), 2941 (br, C–H stretch). ESI MS (*m/z*): 452.0748 (452.08 Calcd for $[C_{17}H_{23}N_7S_2Cu]^+$). Elemental Anal. Calcd (found) for $[C_{19}H_{23}Cu_1N_7S_2]_2[CuCl_4]\cdot 3H_2O$: C, 35.04 (35.14); H, 4.50 (4.10); N, 16.82 (16.67). UV–Vis λ_{max} (CH_3CN)/nm ($\varepsilon/M^{-1}\,cm^{-1}$): 461 (1200), 299 (5100), 258 (34000).

2.2.3. Bis-[(η^3-S,S,N)(2,6-bis){[N-butyl-N′-methylene]triazole-2-thione} pyridinecopper (II) tetrachlorocuprate] (6). In a 25 mL round-bottomed flask, 2,6-bis{[N-butyl-N′-methylene]triazole-2-thione} pyridine (0.1415 g, 0.0003389 moles) was combined with $CuCl_2$ (0.0942 g, 0.000701 moles) and dissolved in dichloromethane (11 mL). The solution mixture was refluxed for 20 h and solvent removed under reduced pressure. Single crystals for X-ray diffraction and elemental analyses were grown by a slow vapor diffusion of diethyl ether into a methanol solution containing the copper complex. Yield: 0.23 g (99%). FT-IR (reflectance, solid crystal, ν_{max}/cm^{-1}, assignment): select IR bands (reflectance, solid crystal), ν_{max}/cm^{-1} (intensity, assignment) 3032(w, C–H stretch), 2955 (br, C–H stretch), 2870 (w, C–H stretch). ESI MS (*m/z*): 480.1064 (480.11 Calcd for $[C_{19}H_{27}N_5S_2Cu]^+$). Elemental Anal. Calcd for $[C_{19}H_{27}CuN_7S_2]_2[CuCl_4]\cdot 2H_2O$: C, 37.92; H, 4.86; N, 16.29. Found: C, 38.32; H, 4.65; N, 16.13. UV–Vis λ_{max} (CH_3CN)/nm ($\varepsilon/M^{-1}\,cm^{-1}$): 461 (1300), 307 (5400), 258 (37000).

2.3. *Crystallographic analyses*

A red-orange, plate-like crystal of **5**, which had dimensions of 0.35 mm × 0.27 mm × 0.15 mm, was secured to a CryoLoop using Paratone oil and placed into the liquid nitrogen stream of a Bruker SMART 1 K diffractometer. Data were collected using graphite monochromated Mo-Kα radiation ($\lambda = 0.71073$ Å) at 203 K in four independent wedges of 606 frames each at phi angles of 0, 90, 180 and 270°. A final set of 50 frames at $\varphi = 0°$ was collected to evaluate the single crystal for indications of decay. No appreciable decay was

found to have occurred after comparison of the measured intensities. All 2474 frames were collected at a width of 0.3°. Data collection and initial indexing were handled using SMART [28]. Frame integration, Lorentz-polarization corrections, and final cell parameter calculations were carried out using SAINT [29]. Multi-scan absorption corrections were performed using SADABS [30]. Space groups were unambiguously assigned by analysis of symmetry and systematic absences determined by XPREP and further verified by PLATON [31, 32]. The structure was solved using direct methods and difference-Fourier techniques. Hydrogens bound to the isopropyl carbons C2, C16, C19, and C33 and to C5, C13, C22, and C30 within the triazole rings were identified using direct methods. All other hydrogens were attached via the riding model at calculated positions. The final structural refinement included anisotropic temperature factors on all non-hydrogen atoms. Structure solution, refinement, graphics, and creation of publication materials were performed using SHELXS, SHELXL, and XSEED [33, 34]. All other pertinent crystallographic details such as h, k, l ranges, 2θ ranges, and R-factors can be found in table 1 (Supplementary material, see online supplemental material at http://dx.doi.org/10.1080/00958972.2014.883070).

A crystal of **6** (*vide infra*) was mounted on a CryoLoop (Hampton Research) and placed in a –100 °C compressed air stream on an Agilent Gemini-EOS Single Crystal Autodiffractometer at Keene State College (Keene, NH). Crystallographic data were collected using graphite monochromated 0.71073 Å Mo-Kα radiation and integrated and corrected for absorption using the *CrysAlisRed* (Oxford Diffraction, 2010 software package) [35]. The structures were solved using direct methods and refined using least-squares on F^2 [36, 37]. All other pertinent crystallographic details such as h, k, l ranges, 2θ ranges, and R-factors can be found in tables 2 or 3 (Supplementary material).

2.4. *Density functional calculations*

Gaussian 03 [38] was used to perform single-point calculations and geometry optimizations using the B3LYP hybrid functional with basis sets as provided with the software. Calculations were performed using *N*-methyl pendant groups and C_2 symmetry in all cases. Structures of the singly cationic imidazolyl- and triazolyl-containing $[(SNS)Cu]^+$ complexes were first optimized in the gas phase to determine a basis set that resulted in molecular structures that matched well with the experimentally determined crystal structures. Structures of the doubly cationic $[(SNS)Cu]^{2+}$ systems were then obtained as part of our electrochemical analysis. Solvent was later added via single-point calculations in the determination of the computed absorption spectra and oxidation potentials. Frequency analyses were performed on the optimized structures to determine whether or not they represented true minima. All structures presented no imaginary frequencies. The calculated IR spectra for the model systems are provided in Supplementary material.

To model the electrochemical experiments, single-point SCRF calculations using DMSO via the CPCM solvent model were performed on the gas-phase optimized structures using the "radii = uff" and "nosymmcav" directives. Oxidation potentials were computed by finding the difference in the total free energies in solution for the neutral and cationic species. These ΔG values were then referenced to the absolute SCE potential in DMSO by subtracting 3.83 V (the established correction to SHE in DMSO) and 0.241 V (the difference between SHE and SCE) [39, 40].

In order to calculate electronic transitions in the UV–Vis region, time-dependent DFT calculations were performed using the B3LYP functional. A solvent model with all of the

same parameters used to compute the oxidation potentials was employed except that acetonitrile was used instead of DMSO.

3. Results and discussion

3.1. *Syntheses*

As shown in scheme 1, ligand precursors **2a**, **3a**, and **3c** react with $CuCl_2$ in refluxing CH_2Cl_2 to afford **4**–**6**. The driving force is the formation of the copper complex, which is sparingly soluble in CH_2Cl_2. Two equivalents of $CuCl_2$ were used to drive the reaction to completion in all cases. All reactions were performed in air and proceeded with yields at or above 64%. Complexes **4**–**6** are orange, soluble in DMSO, acetonitrile, and methanol and

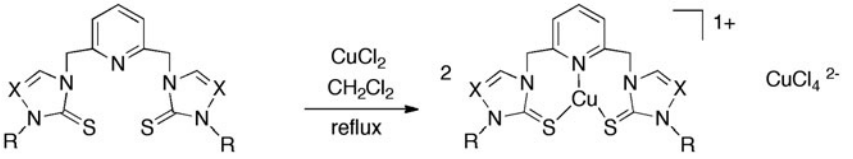

Scheme 1. Preparation of three-coordinate $[(SNS)Cu]^+$ complexes.

are sparingly soluble in dichloromethane and chloroform. Crystals of **5** and **6** suitable for X-ray diffraction were grown by allowing diethyl ether vapor to slowly diffuse into a methanol solution containing the copper complex.

The copper complexes were characterized using single crystal X-ray diffraction (**5** and **6**), UV–Vis spectroscopy (**4**–**6**), electrospray mass spectrometry (**4**–**6**), ATR infrared spectroscopy (**4**–**6**), electron paramagnetic resonance spectroscopy (**4** and **5**), cyclic voltammetry (**4** and **5**), and elemental analysis. (**4**–**6**). The characterizations of these copper complexes are described below.

3.2. *Single crystal X-ray structures*

The solid-state structure of **5** is presented in figure 2. Bond lengths and angles for this compound are summarized in table 2. For this system, as well as for **4** and **6**, disproportionation [41] was observed in the solid state. Two $[(SNS)Cu]^+$ cations and one $[CuCl_4]^{2-}$ anion are present in each unit cell. The elemental analyses for **4**–**6** are consistent with this determination. To probe further this finding, an EPR spectrum of **5** dissolved in frozen methanol solution was acquired at 4 K and will be discussed in a subsequent section.

The solid-state structure of **6** is shown in figure 3 and associated bond lengths and angles are given in table 3. As was observed in **5**, disproportionation gives two $[(SNS)Cu]^+$ and one $[CuCl_4]^{2-}$ in the unit cell for **6**.

Figures 2 and 3 and tables 1 and 2 demonstrate a number of important structural features that **5** and **6** possess. Both molecules exhibit pseudo-trigonal planar geometry about the copper center as reported for other three-coordinate copper(I) complexes [11–23]. The Cu–N bond lengths in each system are approximately 2.0 Å and the Cu–S bonds are 2.2 Å.

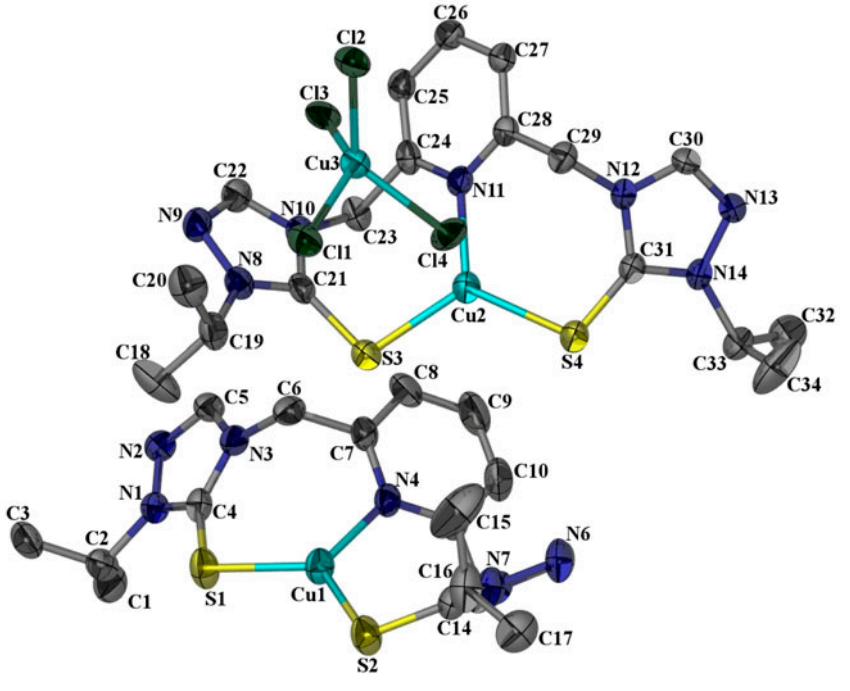

Figure 2. Molecular structure of **5** showing the atom-labeling scheme and 50% probability ellipsoids. The hydrogens have been omitted for clarity.

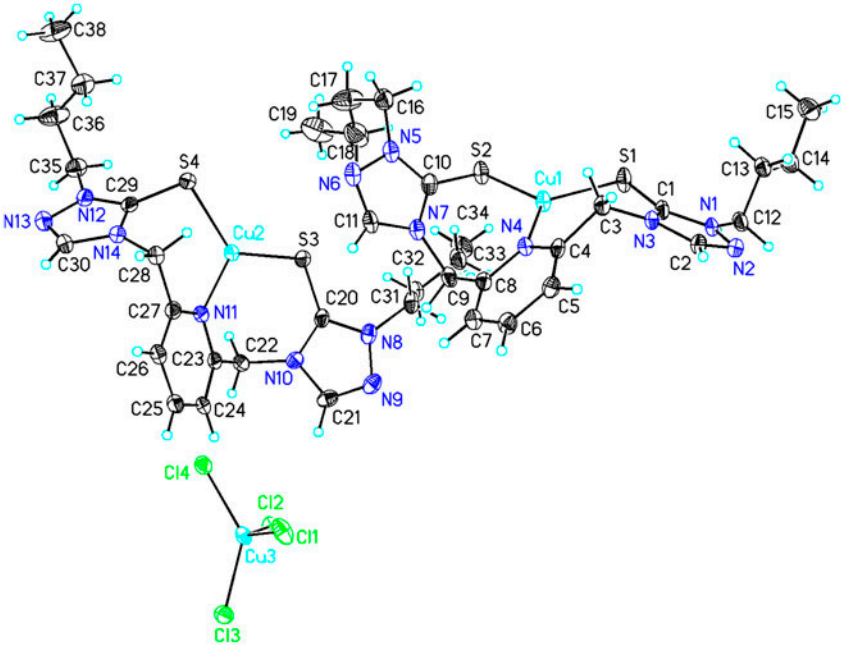

Figure 3. Molecular structure of **6** showing the atom-labeling scheme and 50% probability ellipsoids.

Table 1. Crystal and structure refinement data for **5** and **6**.

	R = *i*Pr (**5**) (X=N)	R = *n*Bu (**6**) (X=N)
Formula	$C_{34}H_{46}Cl_4\ Cu_3N_{14}S_4$	$C_{38}H_{54}Cl_4Cu_3N_{14}S_4$
FW (g/M)	1111.58	1167.61
Temperature (K)	203(2)	173(2)
Wavelength (Å)	0.71073	1.54178
Crystal system	Triclinic	Triclinic
Space group	*P-1*	*P-1*
a (Å)	9.6763(19)	8.7628(6)
b (Å)	12.338(3)	14.7735(10)
c (Å)	21.048(4)	19.8970(13)
α (°)	88.48(3)	102.099(6)
β (°)	77.41(3)	90.808(5)
γ (°)	74.00(3)	90.228(5)
Volume (Å)^3	2355.8(8)	2518.3(3)
Z	2	2
r (Calcd) (g/cm^3)	1.567	1.540
Abs (mm^{-1})	1.789	5.331
F (0 0 0)	1134	1198
Crystal size (mm^3)	0.35 × 0.27 × 0.15	0.12 × 0.10 × 0.06
θ range (°)	1.72–23.41	3.41–71.49
Refl./uniq.	20,435/6866	16,392/9552
R (int)	0.0414	0.0351
Abs correction	Multi-scan	Semi-empirical form equivalents
Max./min.	0.765/0.566	1.00000/0.39117
Ref method	Full matrix least squares on F^2	Full matrix least squares on F^2
Data/restr./par.	6866/0/572	9552/0/573
GOF on F^2	1.024	1.068
R_1 indices ($I > 2s$)	0.0490	0.0881
wR_2	0.1345	0.2502
Peak/hole (e/Å^{-3})	2.04 and –0.46	3.078 and –1.223

Table 2. Selected bond lengths (Å) and angles (°) for **5**.

Cu(1)–S(1)	2.1989(17)
Cu(1)–S(2)	2.2003(17)
Cu(1)–N(4)	2.005(4)
S(1)–C(4)	1.695(6)
S(2)–C(14)	1.696(5)
S(1)–C(6)	1.708(2)
Cu(3)–Cl(1)	2.2343(17)
Cu(3)–Cl(2)	2.2606(16)
Cu(3)–Cl(3)	2.2750(15)
Cu(3)–Cl(4)	2.2507(16)
S(1)–Cu(1)–S(2)	123.63(7)
S(1)–Cu(1)–N(4)	118.86(15)
S(2)–Cu(1)–N(4)	117.49(15)

For **5** and **6**, the Cu–N bond lengths are similar to those reported previously for the three-coordinate copper(I) complexes with trigonal planar geometry [18, 19]. The carbon–sulfur bond lengths in **5** and **6** are between what is normally associated with a C–S single bond (1.83 Å) and a C=S double bond (1.61 Å) [42], ranging from 1.695 to 1.714 Å, meaning that they are closer to a C=S double bond than to a C–S single bond. Furthermore, these Cu–S bond distances are 0.02–0.04 Å shorter than reported by Lobana and co-workers for a thiophosphenyl-bound Cu(I) complex [43].

Also present in the solid-state structures of **5** and **6** is $[CuCl_4]^{2-}$. Inspection of tables 2 and 3 show that the Cu–Cl bond lengths are not all equivalent in this Jahn–Teller distorted

Table 3. Selected bond lengths (Å) and angles (°) for **6**.

Cu(1)–S(1)	2.198(2)
Cu(1)–S(2)	2.225(2)
Cu(1)–N(4)	2.012(6)
S(1)–C(1)	1.702(8)
S(2)–C(10)	1.714(8)
Cu(3)–Cl(1)	2.219(2)
Cu(3)–Cl(1)	2.2343(17)
Cu(3)–Cl(2)	2.293(2)
Cu(3)–Cl(3)	2.235(2)
Cu(3)–Cl(4)	2.235(2)
S(1)–Cu(1)–S(2)	119.92(9)
S(1)–Cu(1)–N(4)	120.54(19)
S(2)–Cu(1)–N(4)	119.51(18)

d^9 anion. The tetrachlorocuprate anion in each structure has a flattened tetrahedral structure as reported previously [44].

Our calculations using the B3LYP functional in Gaussian 03 demonstrate that it is the less expensive basis sets that not only allow for geometry optimizations that provide molecular structures that most closely resemble the experimentally determined X-ray crystal structures, but also provide electronic structure data that fit well with the UV–Vis spectra and the electrochemical data to be presented shortly. The calculations in which the 6-31G (d) basis set was used for the H, C, N, and S atoms and the 6-311G(d,p) basis set employed for Cu result in structures that have Cu–N and Cu–S bond lengths and N–Cu–S and S–Cu–S bond angles that are quite close to those found in the crystal structures. The Cartesian coordinates of the optimized structures determined here and employed in our study are provided in Supplementary material.

3.3. *Electrospray mass spectroscopy*

ESI-MS data for **4**–**6** were collected with cone voltages of 10 and 35 V. The predominant feature in the spectra of **4**–**6** corresponds to the $[(SNS)Cu]^+$ parent ion, indicating that the tridentate ligand remains coordinated to copper during the analysis. For all of these spectra, the isotopic pattern in the mass spectrometry data fits the assigned structure.

3.4. *EPR spectroscopy*

X-band EPR (9.24 GHz) spectroscopy was carried out to complement the single-crystal X-ray diffraction and UV–Vis data presented herein. In figure 4, the low-temperature (10 K) spectra for **4** and **5** are presented. EPR samples of the copper complexes were prepared by dissolving 3 mg of the copper complex in 1 mL of dry methanol. The complexes were stored at room temperature prior to analysis. The spectra were collected through use of a frozen glass after flash-freezing the samples in liquid N_2. Both spectra display typical anisotropic Cu (II) signals with four hyperfine splittings in the lower field region ($g_{||}$) and g values consistent with previously reported copper complexes from the literature [45–48]. For the complexes prepared here, the Cu(II) signal results from the presence of the tetrachlorocuprate.

A locally developed program known as *doublet* [49] was used to simulate the frozen-glass EPR spectrum at 10 K based on the standard spin Hamiltonian of an $S = 1/2$ system. Resonance fields are calculated by diagonalization of the energy matrix. Temperature does not affect the $S = 1/2$ spectra as it affects the high-spin spectra, thus temperature was not

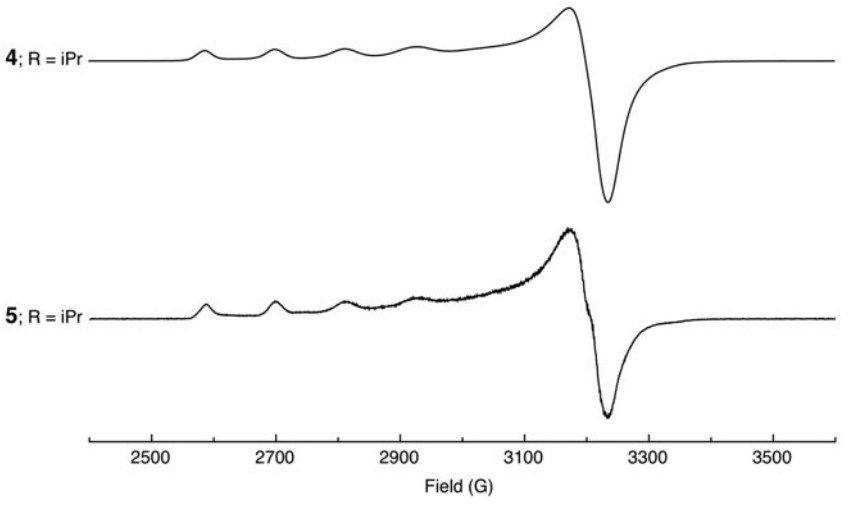

Figure 4. Low temperature (10 K) X-band EPR spectra of oxidized **4** and **5**, measured at 9.24 GHz.

used as a varying parameter in the simulation. The simulation was carried out with different values of g and A until a match was found. The final simulation yielded the parameters g along with the hyperfine structure A, where $g_{\|} = g_z$ and $g_{\perp} = (g_x + g_y)/2$. The simulated line widths of the x, y, and z components are 15, 8, and 35 gauss for **5**, respectively. Simulated parameters are given in table 4 and spectra are given in figure 5.

Complexes **4** and **5** have $g_{\perp}$ and $g_{\|}$ values of 2.09 and 2.43, respectively. The $A_{\|}$ values for **4** and **5** are 11.5 mT and 11.0 mT, respectively. These values are representative of the tetrachlorcuprate. An EPR spectrum of $[CuCl_4]^{2-}$ has been reported previously [50]. The DFT calculations for this anion [50] are consistent with a distorted tetrahedral structure about copper(II). In addition, DFT calculations for the EPR spectrum of a $[CuCl_4]^{2-}$ anion have been reported previously [51]. Rahemi and co-workers [51] calculated $g_{\perp}$ and $g_{\|}$ values of 2.085 and 2.243, respectively, for a $[CuCl_4]^{2-}$ anion with D_2d symmetry with a molecular charge of –2.6.

3.5. *ATR-IR spectroscopy*

ATR-IR spectra were collected for **4**–**6**. All compounds present unique IR spectra. Previously, we reported the C=S stretching frequencies for **1**–**3**, at 1126 cm^{-1} for **1**, 1128 cm^{-1} for **2**, and 1149 cm^{-1} for **3** [1, 2]. These stretches are absent in the corresponding copper complexes. Based on previous reports, the Cu–S and Cu–N stretches should be found at energies less than 470 cm^{-1}, which is below the limit of detection of the IR spectrometer with an ATR cell [52, 53]. Our Gaussian 03 calculations support the assignment of spectral features in this range for the metal–ligand stretches and other motions. For the

Table 4. Simulated EPR parameters for **5**.

Sample	T (K)		g	A (Gauss)
Frozen glass	10	$I = 3/2$ signal	$g_x = 2.0845$ $g_y = 2.0945$ $g_z = 2.4301$	$A_z = 114$

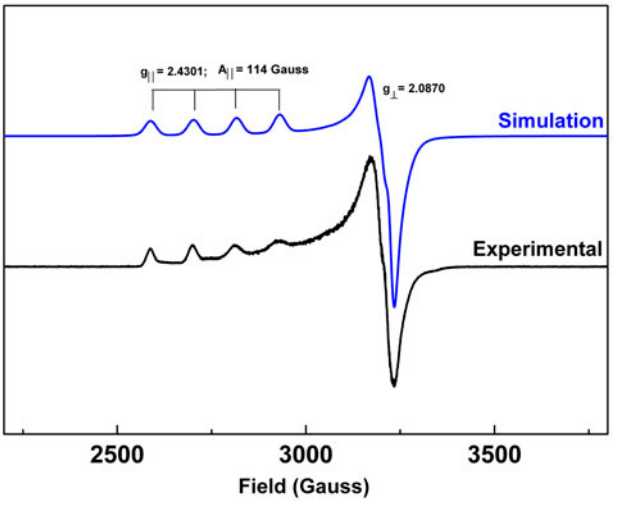

Figure 5. Simulated (blue) and experimental (black) frozen glass EPR spectra of **5** at 9.4 GHz and 10 K (see http://dx.doi.org/10.1080/01694243.2012.735194 for color version).

N-methyl-substituted model for **4**, although a vibrational mode includes Cu–N stretching at 634 cm^{-1} and other stretches in this region include S–Cu–S scissoring and rocking, these motions and Cu–S vibrations dominate the features between 200 and 500 cm^{-1}. Similarly, Cu–N stretching is observed at 632 cm^{-1} for the *N*-methyl-substituted triazolyl systems (model for **5** and **6**) and the various metal–ligand scissoring, rocking, and stretching motions are found between 200 and 560 cm^{-1}. A listing of all calculated molecular motions between 200 and 3400 cm^{-1} for the *N*-methyl-substituted model systems of **4**–**6**, including the relative intensities of the spectral features and descriptions of the motions, is presented in Supplementary material.

3.6. *UV–Vis spectroscopy*

Complexes **4**–**6** were also characterized with UV–Vis spectroscopy. Representative UV–Vis spectra for **4** and **5** are shown in Supplementary material. The spectroscopic features for **4**–**6** are summarized in table 5.

Several electronic transitions are apparent in the UV–Vis spectra of **4**–**6**. All systems exhibit a transition around 460 nm with an extinction coefficient between 200 and

Table 5. Spectroscopic features of **4**–**6**.

Complex	λ (nm)	ε (M^{-1} cm^{-1})
4	462	260
	265	3.6×10^4
	204	4.6×10^4
5	461	1.2×10^3
	299	5.1×10^3
	258	3.4×10^4
6	461	1.3×10^3
	307	5.4×10^3
	258	3.7×10^4

1300 M^{-1} cm^{-1}. Other electronic transitions are present at wavelengths less than approximately 375 nm. Given that each system contains a cationic Cu(I) center as well as Cu(II) in the anion, the UV–Vis spectra of these compounds should represent admixtures of the absorption spectra of two UV–Vis-active species.

Shown in Supplementary material is the UV–Vis spectrum of K_2CuCl_4 collected as part of this work. At 461 nm is an absorption that is also readily apparent in spectra of **4** and **5**. This absorption is, therefore, caused by the tetrachlorocuprate. Several other transitions with maxima at 355, 310, and 258 nm can also be seen. Thiel and co-workers [50] reported absorptions at 200, 258, 311, and 458 nm for $[n\text{BuPy}]_2[CuCl_4]_2$.

Because Gaussian 03 can be used to calculate absorption spectra, we have chosen to use this tool to understand the complex spectra collected here for the $[(SNS)Cu]^+$ complexes. Focusing first on the tetrachlorocuprate anion and using a Jahn–Teller distorted structure for this system with the 6-31G(d) basis set for all atoms, electronic transitions with the strongest computed oscillator strengths (f) are calculated to occur at 454 nm ($f = 0.0126$), 314 nm (0.0423), and 249 nm (0.0539); the shoulder at 355 nm is not found as a distinct feature in the calculated spectrum. Interestingly, using the 6-311G(d, p) basis set for Cu (as was employed in the geometry optimizations) places the lowest energy absorption at 612 nm. We, therefore, have chosen to use the 6-31G(d) basis set for all the atoms in our calculation of the absorption spectra of the imidazolyl- and triazolyl-containing Cu(I)-SNS systems because this basis set gives excellent agreement with the experimentally determined spectrum for $CuCl_4^{2-}$.

Overall, our density functional calculations suggest that the absorptions in the UV–Vis region of $[(SNS)Cu]^+$ systems are obscured by those of the tetrachlorocuprate ion. For the imidazolyl-containing complex, absorptions of strengths similar to those determined for $CuCl_4^{2-}$ are calculated to occur at 446 nm ($f = 0.015$), 382 nm ($f = 0.0408$), 361 nm ($f = 0.0108$), and 347 nm (0.0107), as well as at numerous higher energy wavelengths. In the UV–Vis spectrum of **4**, maximum absorptions are seen at 462 nm, 265 nm, and 204 nm. Contour plots for the molecular orbitals (MOs) involved in the two lowest energy metal–ligand charge transfers are shown in figure 6. In both of these transitions, an electron

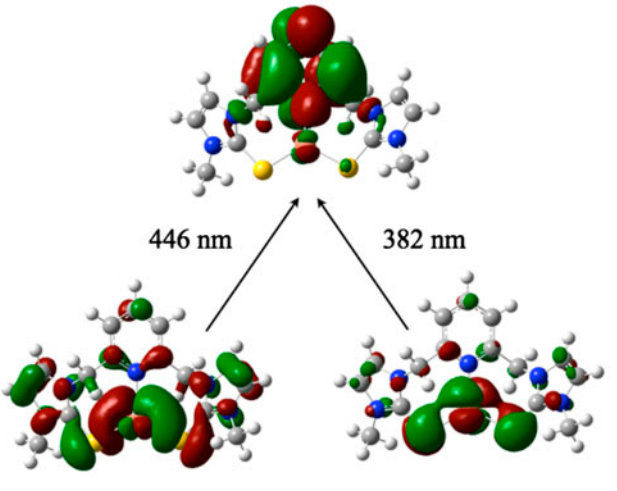

Figure 6. Contour plots of MOs responsible for the absorptions calculated to occur at 446 nm and 382 nm for the *N*-methyl-substituted, imidazolyl-containing $[(SNS)Cu]^+$ system.

is promoted from an MO with significant Cu and S character to one that is largely based on the two-node π system of the pyridinyl unit. The lower energy transition is from the second highest occupied MO (SHOMO) to the LUMO, while the higher energy transition is from the fourth highest occupied MO to the LUMO. Other absorptions in this region, including the HOMO–LUMO transition are calculated as having much weaker oscillator strengths. For the triazolyl-based system, the analogous transitions are calculated to occur at 435 nm ($f = 0.0142$), 375 nm ($f = 0.0117$), and lower wavelengths. In the UV–Vis spectrum of **5**, maximum absorptions are seen at 461 nm, 299 nm, and 258 nm. Given that these wavelengths are in the region where $[CuCl_4]^{2-}$ absorbs, substituting this anion with one that does not absorb in this area of the spectrum will be necessary to locate experimentally the absorptions of the $[(SNS)Cu]^+$ systems. Current efforts are focusing on exchanging the counteranions in the copper complexes.

3.7. *Cyclic voltammetry*

Complexes **4** and **5** were studied by cyclic voltammetry in DMSO as part of their characterizations. The cyclic voltammogram for **4** (Supplementary material) shows oxidation features at 368 and 904 mV, and reduction waves at –43 and –1974 mV, respectively. The cyclic voltammogram for **5** (Supplementary material) shows oxidation features at 452 and 1111 mV, and a reduction wave at –1799 mV. For both systems, the oxidation and reduction waves are broad. Previously, we reported that **2** shows oxidation features at 976 and 1339 mV and **3** shows a single oxidation feature at 1178 mV [2]. As such, the electrochemical profiles presented here are more complex than what we have observed previously [2].

The oxidation process can be modeled computationally by comparing the energies of the optimized structures of $[(SNS)Cu]^+$ and $[(SNS)Cu]^{2+}$ to obtain calculated oxidation potentials. As for calculations of the absorption spectra, using the 6-31G(d) basis set for all atoms gave results that were close to those found experimentally. For the imidazolyl- and triazolyl-based $[(SNS)Cu]^+$ complexes, oxidations are computed to occur at 830 mV and 1076 mV, respectively. We believe that these oxidations represent those found experimentally for **4** and **5** at 904 mV and 1111 mV, respectively, which would indicate removal of an

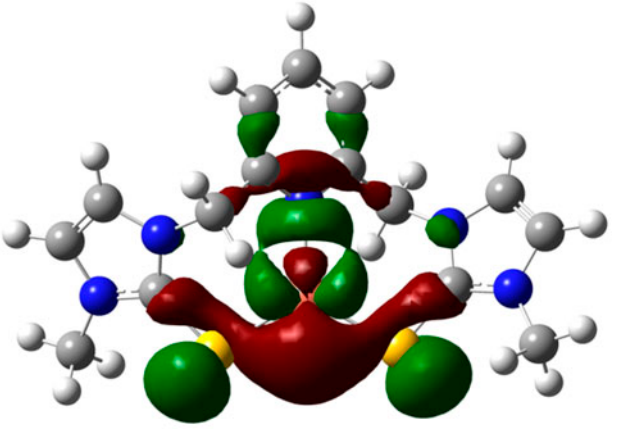

Figure 7. Contour plot of the Cu-, N-, and S-based HOMO of the imidazolyl-based $[(SNS)Cu]^+$ complex.

electron from a predominantly Cu-, N-, and S-based HOMO such as that depicted in figure 7 for the imidazolyl-based $[(SNS)Cu]^+$ complex. We also note that the difference in potentials between the computed oxidations is 246 mV, while that between the experimentally observed oxidations is similar (207 mV) and that the potentials are calculated properly relative to each other. As for the other features present in the experimentally determined cyclic voltammograms, their origin is likely more complex with the presence of the paramagnetic tetrachlorocuprate anion that could be interacting with the $[(SNS)Cu]^{2+}$ cation. We have noted previously [54] the likelihood of intermolecular disulfide bond formation upon oxidation especially for the triazolyl-containing ligand and, therefore, postulate that similar reactions could be occurring here. For example, owing to the Cu–S σ-bonding character of this MO, removal of an electron from this orbital would be expected to weaken the Cu–S bond, thereby allowing the S to detach and react with any active species present.

4. Conclusion

A series of SNS-coordinated Cu(I) compounds have been prepared and characterized through the use of imidazolyl- and triazolyl-based tridentate ligand systems. The three-coordinate copper complexes possess pseudo-trigonal planar geometry at the metal center. Our X-ray crystal structures, supported by elemental analysis, clearly indicate that disproportionation occurs during the formation of these systems resulting in tetrachlorocuprate. The EPR spectra of these systems are consistent with typical anisotropic Cu(II) signals with four hyperfine splittings in the lower field region ($g_{||}$) and g values consistent with previously reported copper complexes. In the electronic spectra, various charge-transfer transitions are apparent and we believe that the absorptions of the $[(SNS)Cu]^+$ complexes are coincident with those of $[CuCl_4]^{2-}$. The cyclic voltammograms do indicate a feature related to the oxidation of $[(SNS)Cu]^+$, but also indicate other redox activity occurring likely as a result of the presence of the tetrachlorocuprate anion, as well as the functional groups of the tridentate ligand systems and related decomposition.

Supplementary material

The ESI-MS, UV–Vis, ATR-IR, and EPR spectra of **4**–**6** are provided. Crystallographic details of **5** and **6** are also given. The Cartesian coordinates of all the optimized structures provided by density functional theory are also provided. In addition, the calculated IR spectra for the model systems are provided in Supplementary material. CCDC files 835944 and 955913 contain the supplementary crystallographic data for this article. These data can be obtained free of charge from The Cambridge Crystallographic Data Centre via www.ccdc.cam.ac.uk/data_request/cif.

Acknowledgements

JRM and ER would like to acknowledge the NSF for supporting the cCWCS Workshop: Crystallography for Chemists in 2011. JRM would like to thank Prof. L. Kraig Steffen for helpful suggestions. We also thank an anonymous reviewer for helpful comments and suggestions.

Funding

This work was supported by generous funding from The Fairfield University Science Institute (JRM, EEB, KAA, CEV), Fairfield University Start-up Funding (JRM), Fairfield University Research Grants (JRM), Fairfield University Summer Research Kuck Fund (MS, EEB, CEV, and EP), the E. Gerald Corrigan '63 Scholarship (CDG), the Hardiman Scholars Program (MS), and an NTID Faculty Evaluation and Development (FEAD) Grant (MAL). JPJ acknowledges the NSF–MRI program [grant number CHE1039027] for funds to purchase the X-ray diffractometer. JRM and DB also acknowledge the MRI grant program [grant number CHE08539] for the purchase of an EPR spectrometer.

References

[1] J.R. Miecznikowski, W. Lo, M.A. Lynn, B.E. O'Loughlin, A.P. DiMarzio, A.M. Martinez, L. Lampe, K.M. Foley, L.C. Keilich, G.P. Lisi, D.J. Kwiecien, C.M. Pires, W.J. Kelly, N.F. Kloczko, K.N. Morio. *Inorg. Chim. Acta*, **376**, 515 (2011).
[2] J.R. Miecznikowski, W. Lo, M.A. Lynn, S. Jain, L.C. Keilich, N.F. Kloczko, B.E. O'Loughlin, A.P. DiMarzio, K.M. Foley, G.P. Lisi, D.J. Kwiecien, E.E. Butrick, E. Powers, R. Al-Abbasee. *Inorg. Chim. Acta*, **387**, 25 (2012).
[3] W.-G. Jia, Y.-B. Huang, G.-X. Jin. *J. Organomet. Chem.*, **694**, 4008 (2009).
[4] Y. Lu. In *Bio-coordination Chemistry*, L. Que Jr., W.B. Tolman (Eds), Vol. 8, pp. 91–122, Elsevier, Oxford (2004).
[5] For synthetic models for "blue" Type 1 or binuclear CuA electron-transfer centers, see: (a) N. Kitajima, K. Fujisawa, Y. Moro-oka. *Inorg. Chem.*, **29**, 357 (1990); (b) N. Kitajima, K. Fujisawa, M. Tanaka, Y. Moro-oka. *J. Am. Chem. Soc.*, **114**, 9232 (1992); (c) D.W. Randall, S.D. George, P.L. Holland, B. Hedman, K.O. Hodgson, W.B. Tolman, E.I. Solomon. *J. Am. Chem. Soc.*, **122**, 11632 (2000); (d) P.L. Holland, W.B. Tolman. *J. Am. Chem. Soc.*, **122**, 6331 (2000).
[6] P. Chen, S.I. Gorelsky, S. Ghosh, E.I. Solomon. *Angew. Chem., Int. Ed.*, **43**, 4132 (2004).
[7] For recent synthetic models of the N_2OR copper center which are (di)sulfido-copper complexes, see: (a) E.C. Brown, N.W. Aboelella, A.M. Reynolds, G. Aullón, S. Alvarez, W.B. Tolman. *Inorg. Chem.*, **43**, 3335 (2004); (b) E.C. Brown, J.T. York, W.E. Antholine, E. Ruiz, S. Alvarez, W.B. Tolman. *J. Am. Chem. Soc.*, **127**, 13752 (2005); (c) J.T. York, E.C. Brown, W.B. Tolman. *Angew. Chem., Int. Ed.*, **44**, 7745 (2005); (d) M.E. Helton, P. Chen, P.P. Paul, Z. Tyeklár, R.D. Sommer, L.N. Zhakarov, A.L. Rheingold, E.I. Solomon, K.D. Karlin. *J. Am. Chem. Soc.*, **125**, 1160 (2003); (e) M.E. Helton, D. Maiti, L.N. Zhakarov, A.L. Rheingold, J.A. Porco, K.D. Karlin. *Angew. Chem., Int. Ed.*, **45**, 1138 (2006).
[8] Y. Lee, A.A.N. Sarjeant, K.D. Karlin. *Chem. Commun.*, **6**, 621 (2006).
[9] E.I. Solomon, R.K. Szilagyi, S.D. DeBeer George, L. Basumallick. *Chem. Rev.*, **104**, 419 (2004).
[10] D.B. Rorabacher. *Chem. Rev.*, **104**, 651 (2004).
[11] V.A. Krylova, P.I. Djurovich, J.W. Aronson, R. Haiges, M.T. Whited, M.E. Thompson. *Organometallics*, **31**, 7983 (2012).
[12] C.C. Chou, H.-J. Liu, L. Chao, H.-C. Syu, T.-S. Kuo. *Polyhedron*, **37**, 60 (2012).
[13] M. Hashimoto, S. Igawa, M. Yashima, I. Kawata. *J. Am. Chem. Soc.*, **133**, 10348 (2011).
[14] T.S. Singh Lobana, P.S. Kumari, R. Sharma, A. Castineiras, R.J. Butcher, T. Akitsu, Y. Aritake. *Dalton Trans.*, 3219 (2011).
[15] C.C. Chou, H.-J. Liu, L.H.-C. Chao. *Chem. Commun.*, 6382 (2009).
[16] B.A. Gandhi, O. Green, J.N. Burstyn. *Inorg. Chem.*, **46**, 3816 (2007).
[17] M.A.S. Gohera, T.C.W. Mak. *Polyhedron*, **17**, 3485 (1998).
[18] M. Munakata, M. Maekawa, S. Kitagawa, S. Matsuyama, H. Masuda. *Inorg. Chem.*, **28**, 4300 (1989).
[19] T.N. Sorrell, M.R. Malachowski. *Inorg. Chem.*, **22**, 1883 (1983).
[20] J.A. Tiethof, A.T. Hetey, D.W. Meek. *Inorg. Chem.*, **13**, 2505 (1974).
[21] J.A. Tiethof, A.T. Hetey, P.E. Nicpon, D.W. Meek. *Inorg. Nucl. Chem. Lett.*, **8**, 841 (1972).
[22] F. Kiyoshi, N. Yuki, M. Yoshitaro, O. Ken-Ichi, L. Nicolai. *Inorg. Chem.*, **46**, 10607 (2007).
[23] C.G. Palvan, S. Ramaprabhu. *J. Chem. Soc., Dalton Trans.*, 3513 (2000).
[24] B.A. Jazdzewski, P.L. Holland, M. Pink, V.G. Young, D.J.E. Spencer, W.B. Tolman. *Inorg. Chem.*, **40**, 6097 (2001).
[25] P.J. Chmielewski. *Angew. Chem., Int. Ed.*, **49**, 1359 (2010).
[26] S. Saito, K. Furukawa, A. Osuka. *Angew. Chem., Int. Ed.*, **48**, 8086 (2009).
[27] P.L. Holland, W.B. Tolman. *J. Am. Chem. Soc.*, **121**, 7270 (1999).
[28] W. Zhong, M. Xie, Q. Jiang, Y. Li, H. Yan. *Chem. Commun.*, **48**, 2152 (2012).

[29] Bruker Analytical X-ray Systems, *SMART, Software for the CCD Detector System*, Version 5.050 (NT), Madison, WI, USA (1998).
[30] Bruker Analytical X-ray Systems, *SAINT, Software for the CCD Detector System*, Version 5.01 (NT), Madison, WI, USA (1998).
[31] R.H. Blessing. *Acta Crystallogr., Sect. A: Found: Crystallogr.*, **51**, 33 (1995).
[32] G.M. Sheldrick. *XPREP, Program for Space Group Determination*, University of Göttingen, Germany (1996).
[33] A.L. Speck. *PLATON, A Multipurpose Crystallographic Tool*, Utrecht University, The Netherlands (2001).
[34] G.M. Sheldrick. *SHELXS-97, Program for Crystal Structure Determination*, University of Göttingen, Germany (1997).
[35] L.J. Barbour. *J. Supramol. Chem.*, **1**, 189 (2001).
[36] Oxford Diffraction. *CrysAlis PRO and CrysAlis RED*, Oxford Diffraction Ltd., Oxfordshire, England (2010).
[37] G.M. Sheldrick, *Acta Crystallogr., Sect. A: Found: Crystallogr.*, **64**, 112 (2008).
[38] M.J. Frisch, G.W. Trucks, H.B. Schlegel, G.E. Scuseria, M.A. Robb, J.R. Cheeseman, J.A. Montgomery, Jr., T. Vreven, K.N. Kudin, J.C. Burant, J.M. Millam, S.S. Iyengar, J. Tomasi, V. Barone, B. Mennucci, M. Cossi, G. Scalmani, N. Rega, G.A. Petersson, H. Nakatsuji, M. Hada, M. Ehara, K. Toyota, R. Fukuda, J. Hasegawa, M. Ishida, T. Nakajima, Y. Honda, O. Kitao, H. Nakai, M. Klene, X. Li, J.E. Knox, H.P. Hratchian, J.B. Cross, V. Bakken, C. Adamo, J. Jaramillo, R. Gomperts, R.E. Stratmann, O. Yazyev, A.J. Austin, R. Cammi, C. Pomelli, J.W. Ochterski, P.Y. Ayala, K. Morokuma, G.A. Voth, P. Salvador, J.J. Dannenberg, V.G. Zakrzewski, S. Dapprich, A.D. Daniels, M.C. Strain, O. Farkas, D.K. Malick, A.D. Rabuck, K. Raghavachari, J.B. Foresman, J.V. Ortiz, Q. Cui, A.G. Baboul, S. Clifford, J. Cioslowski, B.B. Stefanov, G. Liu, A. Liashenko, P. Piskorz, I. Komaromi, R.L. Martin, D.J. Fox, T. Keith, M.A. Al Laham, C.Y. Peng, A. Nanayakkara, M. Challacombe, P.M.W. Gill, B. Johnson, W. Chen, M.W. Wong, C. Gonzalez, J.A. Pople. *Gaussian 03, Revision E.01*, Gaussian, Inc., Wallingford, CT (2004).
[39] W.R. Fawcett. *Langmuir*, **24**, 9868 (2008).
[40] L.E. Roy, E. Jakubikova, G. Guthrie, E.R. Batista. *J. Phys. Chem. A*, **1**, 6745–6750 (2009).
[41] S.F. Hannigan, J.S. Lum, J.W. Bacon, C. Moore, J.A. Golen, A.L. Rheingold, L.H. Doerrer. *Organometallics*, **32**, 3429 (2013).
[42] B.V. Trzhtsinskaya, N.D. Abramova. *J. Sulfur Chem.*, **10**, 389 (1991).
[43] T.S. Lobana, G. Singh, T. Nishioka. *J. Coord. Chem.*, **57**, 955 (2004).
[44] V. Fernandez, M. Moran, M.T. Gutierrez-Rios, C. Foces-Foces, F.H. Cano. *Inorg. Chim. Acta*, **128**, 239 (1987).
[45] S. Nellutla, J. van Tol, N.S. Dalal, L.H. Bi, U. Kortz, B. Keita, L. Nadjo, G.A. Khitrov, A.G. Marshall. *Inorg. Chem.*, **44**, 9795 (2005).
[46] J.A. Weil, J.R. Bolton, J.E. Wertz, J.A. Nugent. *Electron Paramagnetic Resonance: Elementary Theory and Practical Applications*, p. 68, Wiley, New York, NY (1994).
[47] R.L. Carlin. *Magnetochemistry*, p. 314, Springer-Verlag, Heidelberg (1986).
[48] A. Winter, A. Zabel, P. Strauch. *Int. J. Mol. Sci.*, **13**, 1612 (2012).
[49] A. Ozarowski. *Doublet*, National High Magnetic Field Laboratory, Tallahassee, FL.
[50] K. Thiel, T. Klamroth, P. Strauch, A. Taubert. *Phys. Chem. Chem. Phys.*, **13**, 13537 (2011).
[51] H. Rahemi, S.F. Tayyari, M.J. Riley. *J. Theor. Comput. Chem.*, 7, 53 (2008).
[52] F.S. Parker. *Applications of Infrared, Raman, and Resonance Raman Spectroscopy in Biochemistry*, p. 300, Plenum Press, New York, NY (1983).
[53] M.E. Helton, P. Chen, P.P. Paul, Z. Tyeklár, R.D. Sommer, L.N. Zakharov, A.L. Rheingold, E.I. Solomon, K.D. Karlin. *J. Am. Chem. Soc.*, **125**, 1160 (2003).
[54] J.R. Miecznikowski, J.P. Jasinski, M.A. Lynn, S.S. Jain, E.E. Butrick, A.E.R. Drozdoski, K.A. Archer, J.T. Panarra. *Inorg. Chim. Acta*, **394**, 310 (2013).